PRAMANA
— journal of
physics

Vol. 61, No. 1
July 2003
pp. 141–152

Superiority of Bessel function over Zernicke polynomial as base function for radial expansion in tomographic reconstruction

A K CHATTOPADHYAY and C V S RAO
Institute for Plasma Research, Bhat, Gandhinagar 382 428, India
Email: asim@ipr.res.in

MS received 7 December 2002; accepted 1 April 2003

Abstract. Here we describe the superiority of Bessel function as base function for radial expansion over Zernicke polynomial in the tomographic reconstruction technique. The causes for the superiority have been described in detail. The superiority has been shown both with simulated data for Kadomtsev's model for saw-tooth oscillation and real experimental x-ray data from W7-AS Stellarator.

Keywords. Soft x-ray tomography; tokamak; Kadomtsev's model; MHD mode.

PACS Nos 87.59.Fm; 52.55.Tn; 52.55.Fa; 52.70.La

1. Introduction

Soft x-ray (sxr) tomography is a non-invasive diagnostic tool mainly used to study MHD phenomena in tokamak plasma. Its use as a technique to measure plasma density, temperature and impurity concentration on routine basis has been proven [1–6]. Other functions such as determination of position and control of shape of the plasma and determination of radial current distribution [7,8] have been demonstrated more as capabilities than as a technique to use on routine basis.

Soft x-ray diagnostic gives line integrated measurement by the detector. Practically each detector sees the plasma through a cone of small solid angle due to finite exposed surface area of the detector and the axis of this cone is designated as *chord*. Each chord is defined by (p, ϕ) where p is the perpendicular distance of the chord from the plasma centre and ϕ, the angle measured from the positive x-axis as shown in figure 1.

Mathematically, the tomography problem consists of solving the system of integral equations [3–5]

$$\int_s f(p,\phi) = \int_{L_s} g(r,\theta)\mathrm{d}L, \quad s = 1, 2, \ldots, M$$

where $f(p,\phi)$ is the x-ray chord brightness in (W/m^2/Sr) and $g(r,\theta)$ is the local emissivity in (W/m^3/Sr). The integral is along the line-of-sight (figure 1) and M is the number

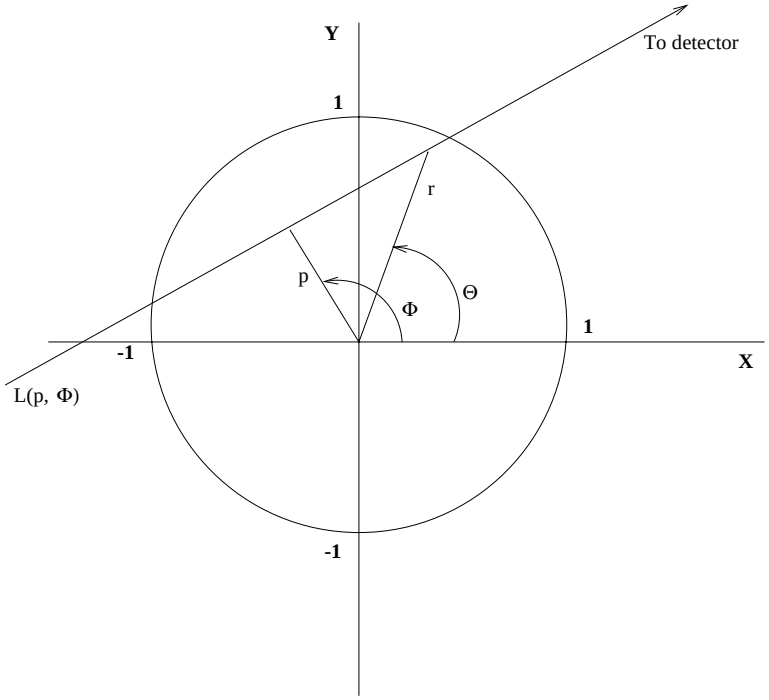

Figure 1. Detectors integrate the local emissivity, $g(r,\theta)$ along lines-of-sight, L defined by (p,ϕ). The emitting region must be completely contained within the circular region.

of available measurements. This system of inhomogeneous Fredholm equations of first kind [9], is always undetermined, since an infinite number of measurements f_s would be required to determine g exactly. But due to space constraints the number of line integrated data available in fusion research is usually of the order of 10^2, whereas that in medical tomography is of the order of 10^5.

Various mathematical methods have been developed to perform tomographic reconstructions of objects which emit or absorb x-rays. The schemes for obtaining reconstruction can be broadly divided into two categories, viz. finite element method and analytical method. Discussion of finite element method is out of scope of this paper. In analytical method if we choose polar coordinates, a Fourier decomposition for the angular part and a polynomial expansion for the radial part of g can be used. The underdetermined system of integral equations is thus transformed to an overdetermined system of algebraic equations which can be solved for the coefficients of the base functions using a *least-square fit*. Such solutions are provided by Cormack using Zernicke polynomial as the base function [10,11] and by Wang and Granetz using Bessel function of first kind as the base function [12,13] for the radial part. In this paper, we shall compare the two methods and show the superiority of the Bessel function as base function.

The structure of the paper is as follows: Section 2 describes the mathematical method. Section 3 deals with the test of the two methods with simulated and experimental data. Conclusion of this work has been drawn in §4.

2. Mathematical method

In §1, it has been shown that the integral measured by each detector can be written as

$$f(p,\phi) = \int_{L(p,\phi)} g(r,\theta)\, \mathrm{d}l \tag{1}$$

where $g(r,\theta)$ is the plasma emissivity and $f(p,\phi)$ is the brightness. The emitting region, which may have a cross-section of any arbitrary shape, is assumed to be lying in a circle of radius normalized to unity. The local emission is to be reconstructed over this area, specified by $0 \le r \le 1$ and $0 \le \theta \le 2\pi$.

The 2D quantities in eq. (1) are decomposed into their Fourier harmonic components to take care of the angular parts. Let

$$g(r,\theta) = \sum_{m=0}^{\infty} [g_m^c(r)\cos(m\theta) + g_m^s(r)\sin(m\theta)], \tag{2}$$

$$f(p,\phi) = \sum_{m=0}^{\infty} [f_m^c(p)\cos(m\phi) + f_m^s(p)\sin(m\phi)] \tag{3}$$

with radial part expanded as

$$g_m^{c,s}(r) = \sum_{l=0}^{\infty} a_{m,l}^{c,s}\, g_{m,l}(r). \tag{4}$$

Substituting these expansions in eq. (2), we get

$$f_m^{c,s}(p) = \sum_{l=0}^{\infty} a_{m,l}^{c,s}\; f_{m,l}(p), \tag{5}$$

where $f_{m,l}(p)$ is related to $g_{m,l}(r)$ by the equation [14,15]

$$f_{m,l}(p) = 2\int_p^1 \frac{g_{m,l}(r) T_m(p/r) r\,\mathrm{d}r}{\sqrt{(r^2-p^2)}}, \tag{6}$$

where $T_m(x) = \cos\{m\cos^{-1}(x)\}$ is the Chebyshev polynomial of the first kind. Once $g_{m,l}(r)$ is chosen and hence $f_{m,l}(p)$ is calculated from eq. (6), eq. (3) can be approximately truncated and a least square fit to the data determines $a_{m,l}^{c,s}$. The coefficients are then substituted in (2) to obtain the desired function $g(r,\theta)$.

Cormak [10,11] expanded $g_{m,l}(r)$ in terms of the complete set of orthogonal functions known as Zernicke polynomial, $R_m^l(r)$ so that

$$g_m^l(r) = R_m^l(r), \tag{7}$$

where

$$R_m^l(r) = \sum_{s=0}^{l} \frac{(-1)^s (m+2l-s)!}{s!(m+l-s)!(l-s)!} r^{(m+2l-2s)}. \tag{8}$$

The substitution of eq. (7) in (6) yields a surprisingly simple expression of the expansion of $f_{m,l}(p)$ [10,11] in analytical form as shown below:

$$f_{m,l}(p) = \frac{2}{(m+2l+1)} \sin\{(m+2l+1)\cos^{-1}(p)\}. \tag{9}$$

So,

$$f_m^{c,s}(p) = \sum_{l=0}^{\infty} a_{m,l}^{c,s} \frac{2}{(m+2l+1)} \sin\{(m+2l+1)\cos^{-1}(p)\}. \tag{10}$$

The above expansion for $f_m^{c,s}(p)$ is substituted into eq. (3) to get the result in double summation:

$$f(p,\phi) = \sum_{m=0}^{\infty}\sum_{l=0}^{\infty}\left[a_{m,l}^{c}\frac{2}{(m+2l+1)}\sin\{(m+2l+1)\cos^{-1}(p)\}\right]\cos(m\phi) + \sum_{m=0}^{\infty}\sum_{l=0}^{\infty}\left[a_{m,l}^{s}\frac{2}{(m+2l+1)}\sin\{(m+2l+1)\cos^{-1}(p)\}\right]\sin(m\phi). \tag{11}$$

Wang and Granetz [12,13] used Fourier–Bessel expansion to represent the source function, $g_{m,l}(r)$, i.e.,

$$g_{m,l}(r) = J_m(x_{m,l}\, r), \tag{12}$$

where $x_{m,l}$ is the lth zero of the mth order Bessel function, $J_m(z)$. Now putting (12) in (6) leads to

$$f_{m,l}(p) = 2\int_p^1 \frac{J_m(x_{m,l}\, r)\; T_m(p/r) r\,\mathrm{d}r}{\sqrt{(r^2-p^2)}}. \tag{13}$$

But to perform the integration of eq. (13), a tricky algorithm is required to avoid the singularity at $r = p$ and computation is time-consuming. To overcome this, Wang and Granetz [12] have reduced (13) to the following simpler form:

$$f_{m,l}(p) = -2J'_m(x_{m,l}) \int_0^{\cos^{-1}p}\left[\mathrm{d}\theta\cos(m\theta)\sin\{x_{m,l}(\cos\theta - p)\}\right]. \tag{14}$$

Since the integrand is written in terms of sinusoidal functions, calculation has become substantially faster. However, they [13] further simplified it to avoid the integration and obtained the following analytical series expression [12]

$$f_{m,l}(p) = -2J'_m(x_{m,l}) \sum_{n=0,\; n\neq m}^{\infty} \delta_n J_n(x_{m,l}) \sin(n\pi/2 - x_{m,l}p) \times \left[\frac{\sin\{(m+n)\cos^{-1}p\}}{(m+n)} + \frac{\sin\{(m-n)\cos^{-1}p\}}{(m-n)}\right] \tag{15}$$

or in compact form:

$$f_{m,l}(p) = -2\sqrt{(1-p^2)}J'_m(x_{m,l}) \sum_{n=0,\ n\neq m}^{\infty} \delta_n J_n(x_{m,l}) \sin(n\pi/2 - x_{m,l}p) \times \left[\frac{U_{m+n-1}(p)}{(m+n)} + \frac{U_{m-n-1}(p)}{(m-n)}\right], \quad (16)$$

where $\delta_n = 1/2$ for $n = 0$ and $\delta_n = 1$ otherwise, and $U_m(p) = \sin[(m+1)\cos^{-1}(p)]/\sqrt{(1-p^2)}$ is the Chebyshev polynomial of second kind. The problem reduces to finding the a_{ml}^{cs} coefficients. An efficient way of doing this is to substitute $f_m^{cs}(p)$ in eq. (5) into eq. (3) which results in a double sum of the form

$$f(p,\phi) = \sum_{m=0}^{\infty}\sum_{l=0}^{\infty}(a_{ml}^{c}\cos\ m\phi + a_{ml}^{s}\sin\ m\phi) \times \left[-2\sqrt{(1-p^2)}J'_m(x_{m,l}) \sum_{n=0,\ n\neq m}^{\infty} \delta_n J_n(x_{m,l}) \sin(n\pi/2 - x_{m,l}p) \times \left\{\frac{U_{m+n-1}(p)}{(m+n)} + \frac{U_{m-n-1}(p)}{(m-n)}\right\}\right]. \quad (17)$$

Equations (11) and (17) which are found by Cormack and Granetz and Wang respectively by choosing the different base functions for radial expansion must be truncated at some maximum values of m and l in order to solve for the unknowns. Equation (11) or eq. (17) is a linear expansion of $f(p,\phi)$ into a finite number of terms representing 2D surfaces, each of which has an unknown coefficient. If $f(p,\phi)$ is measured along M different chords, then we obtain M independent linear equations which can be written in matrix form as follows:

$$a\,W = f.$$

The elements of W matrix depend only on the detector geometry and the number of angular and radial harmonics which are used to fit the data. If these do not change, then the whole matrix can be calculated once. As long as the number of detectors M exceeds the number of unknown coefficients a_{ml}^{cs}, one can arrive at a solution for these unknowns in the least squares sense by a simple and efficient matrix multiplication:

$$a = W^{-1}\cdot f.$$

These coefficients are then used in eq. (4) to get $g_m^{(c,s)}(r)$. These Fourier emission harmonics are then summed up in eq. (2) to give the total reconstructed image.

3. Test of the reconstructed images

Two tomographic codes, one using Zernicke polynomial as the base function and the other using Bessel function as the base function for radial expansion have been prepared from eqs (11) and (17) respectively [16]. While comparing Zernicke polynomial and Bessel function in the light of their use as base function for radial expansion in tomographic reconstruction technique, there are some obvious drawbacks in using the Zernicke polynomial. In our assumption the emissivity is zero at the boundary, i.e., on and outside the unit circle. However, Zernicke polynomial is not zero at the boundary as shown in figure 2b. This is the first problem in Cormack inversion. It has l zeros in $(0,1)$, and the density of zeros is

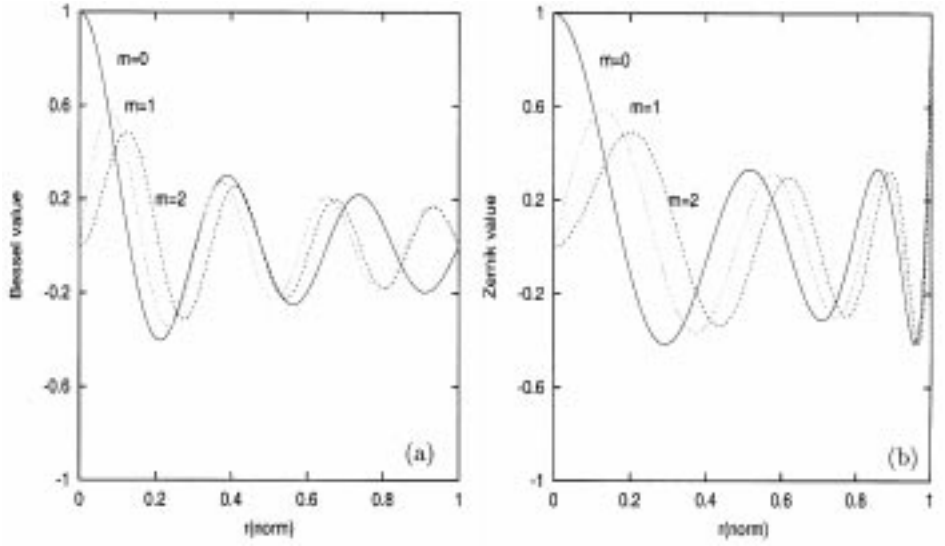

Figure 2. (**a**) The Bessel function with $l = 6$ and $m = 0, 1, 2$. (**b**) The Zernicke polynomial for the same l and m values. Note the boundary values of the two functions. For details, see text.

higher near the boundary than close to the centre. When the emissivity profile has a fine structure near the centre, which appear in the soft x-ray measurements, this character is inconvenient. Therefore, when the Cormack method is applied to the soft x-ray tomography a number of terms should be taken into account, which is the second problem. Indirectly this enhances the soft x-ray cost also. But when we use the Bessel function as a base function, it solves most of the problems arising due to the use of the Zernicke polynomials. The character that Bessel function, $J_m(x_{m,l}r)$, is zero at the boundary is consistent with our assumption that emissivity will be zero at the boundary. Figure 2a shows that at the edge the values of the Bessel function are zero. $J_m(x_{m,l}r)$ has l zeros in $(0,1)$, and the density of zeros is almost uniform in $(0,1)$. Therefore, expansion terms are much less than those of the Cormack inversion.

In earlier works using Zernicke polynomial, fictitious chords were introduced at the edge and the brightness values were set to zero. This introduces distortions to tomographic pictures and reduces the reliability of interpretations of the emissivity at the plasma centre where fine structure has been observed [2]. This uncertainty in interpretation disappears when Bessel function is used as a base function, since the zeros of Bessel function are chosen in such a fashion that the Bessel value is zero on the boundary.

The superiority of Bessel function as base function over Zernicke polynomial has been shown below taking simulated data for Kadomtsev's model for saw-tooth oscillation and experimental data from W7-AS Stellarator.

3.1 *Testing with simulated data*

For testing with simulated data we have chosen a configuration of 7 arrays with 115 detectors around poloidal locations of our upcoming steady state superconducting tokamak,

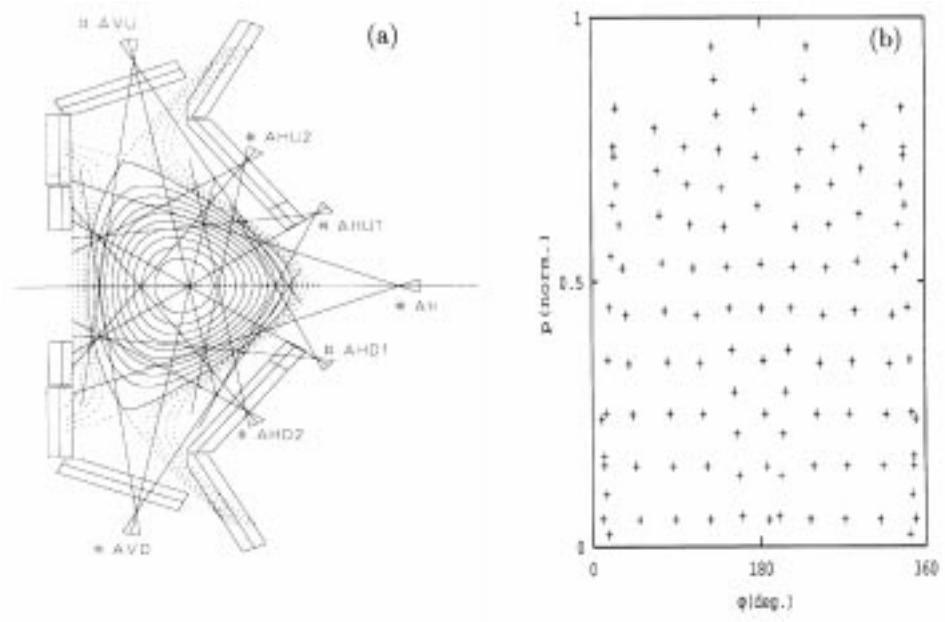

Figure 3. (**a**) The arrangement of 7 fan arrays to be installed in SST-1. (**b**) Plot of (p, ϕ)-coordinates of 115 chords in 7 arrays.

SST-1 [16–18] as shown in figure 3a. Figure 3b shows the near optimal (p, ϕ) positions of the detectors of these arrays. The source function [14] in figure 4a exhibits some qualitative features of the Kadomtsev's total reconnection model, i.e., a relatively flat region in the centre and a displaced circular hot core. Figure 4a is the source function for saw-tooth oscillation according to the Kadomtsev's model. Figure 4b is the reconstructed image when Bessel function was used as a base function for radial expansion. The reconstructed image is quite indistinguishable from the source function. The $m = 0, 1, 2$ angular modes and 10 Bessel zeros for $m = 0, 7$ Bessel zeros for $m = 1$ and 4 Bessel zeros for $m = 2$ are used for radial expansion in this reconstruction. No fictitious or virtual chord with zero brightness value has been used at the boundary region. Figure 4c is the reconstructed image when Zernicke polynomial was used as a base function for the radial expansion. The reconstructed image is quite acceptable judging the brightness values at different radial positions with those of the source function. But to get this reconstructed image, 180 virtual chords with zero brightness values have to be put at the edge region. The $m = 0, 1, 2$ angular modes and $l = 10, 8, 7$ radial modes for $m = 0, 1, 2$ respectively are used here, whereas figure 4d shows that the same number of angular modes and Zernicke radial modes without virtual chords could not reconstruct the source function. The spikes at the edge region are easily noticeable. Apart from this, due to the lack of virtual chords reconstructed image at the central region is also highly affected. Figure 5 shows the 3D images of Kadomtsev's model for saw-tooth oscillation when reconstructed with the help of Zernicke polynomial as the base function for radial expansion. Figure 5a is the reconstructed 3D image when 180 virtual chords were used for reconstruction whose 2D image is shown in figure 4c; whereas figure 5b is the 3D image when no virtual chord was used. Huge spikes and small negative

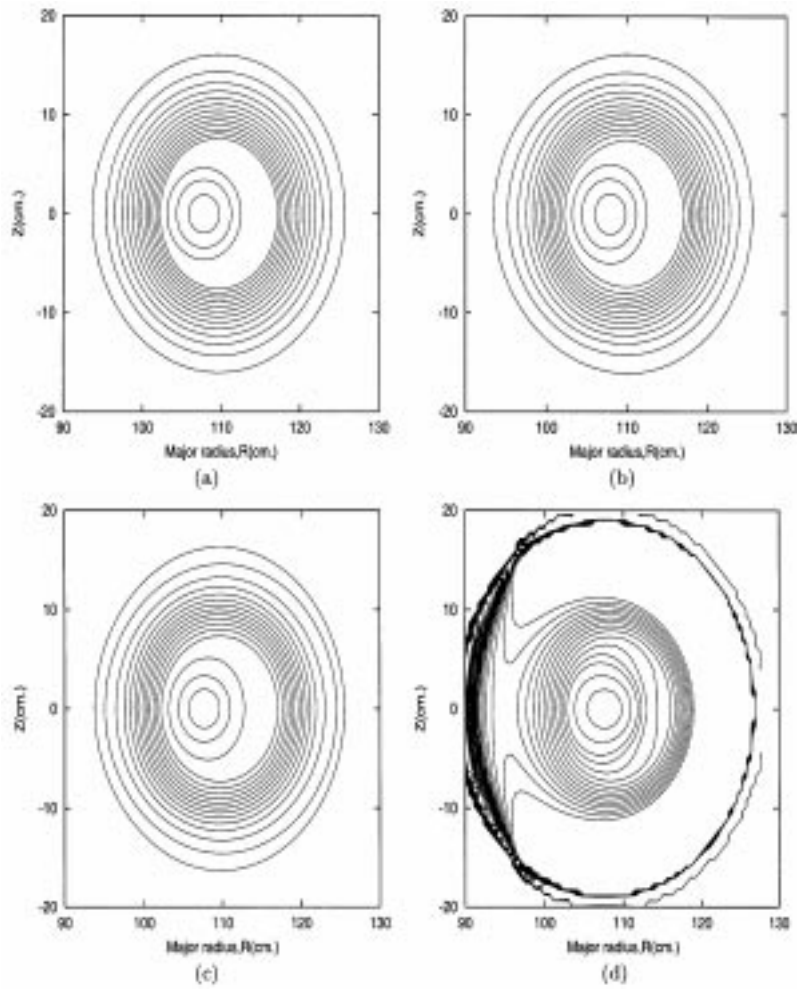

Figure 4. (**a**) The source function for saw-tooth oscillation according to Kadomtsev's model. (**b**) Reconstructed image with Bessel function as the base function for radial expansion with no fictitious or virtual chord. (**c**) Reconstructed image with Zernicke polynomial as the base function for radial expansion using 180 virtual chords. (**d**) The reconstructed image with Zernicke polynomial as the base function when no virtual chord is used. The spikes at the boundary region is evident in (d). For details, see text.

emissivity at the boundary region are obvious from the figure which is the main problem to use the Zernicke polynomial as base function and this comes from the basic nature of the Zernicke polynomial as shown in figure 2.

3.2 *Testing with experimental data*

Soft x-ray data from W7-AS Stellarator [6,15] were taken to test with experimental data. Currently W7-AS Stellarator is an eight-camera soft x-ray tomography system and each

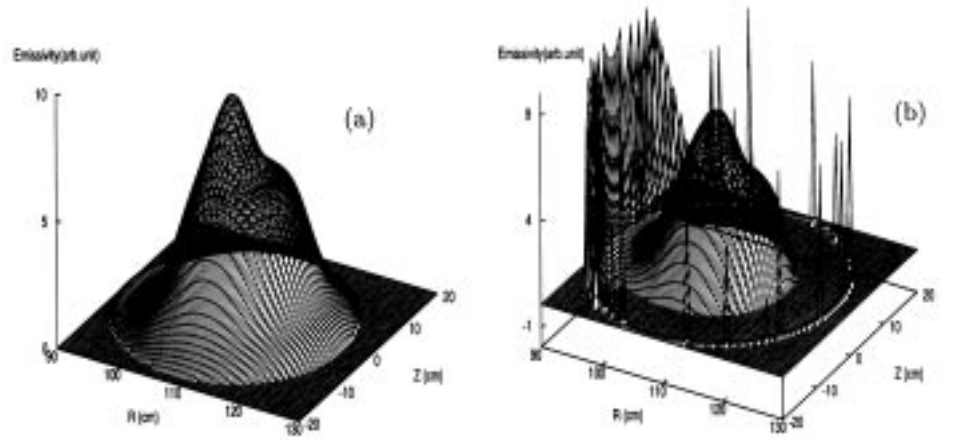

Figure 5. (**a**) The 3D image of Kadomtsev's model for saw-tooth oscillation reconstructed with the code using Zernicke polynomial as the base function for radial expansion when 180 virtual chords were used. (**b**) The 3D image reconstructed with that code when no virtual chord was used. The spikes and small negative emissivity is obvious at the edge region.

camera consists of 32 detectors. The plasma cross-section of W7-AS Stellarator is triangular. Out of the 256 detectors, 13 were bad and were excluded. So, effective number of detectors is 243. Figure 6a shows the reconstructed image of W7-AS Stellarator sxr data when Bessel function was used as the base function for radial expansion. Two hundred and fourty three experimental sxr data, $m = 0, 1, 2, 3, 4$ angular modes and five Bessel zeros for each angular mode were used to reconstruct the image. No virtual chord with zero emissivity was used to reconstruct this image. It takes a total of 45 expansion terms to reconstruct the image. We have scaled our contour plot to the same Z and R scale and compared with those of Weller and Klose [15] who obtained with their code as shown in figure 6c. The positions of the islands have been checked and found to match excellently. Figure 6b is the reconstructed image of W7-AS Stellarator data when Zernicke polynomial was used as a base function. It also matches well with the supplied figure as shown in figure 6c. But to get this reconstructed image 243 experimental sxr data, $m = 0, 1, 2, 3, 4$ angular modes, 7 radial modes of Zernicke polynomial for each angular mode and 249 virtual chords with zero brightness were used. It needs a total of 72 expansion terms to reconstruct the image. Figure 7a is the 3D plot of emissivity of W7-AS Stellarator sxr data done using Bessel function as a base function; whereas figure 7b is that when Zernicke polynomial was used as a base function. Comparison with the supplied 3D plot [15] of sxr intensity as shown in figure 7c shows that on an avarage the agreement is excellent. Both the equilibrium surface and $m = 3$ mode structure can be recovered with both the reconstruction methods. The apparent difference seen between the supplied 3D figure and the reconstructed figures is due to the different viewing angle of the figures.

4. Conclusion

Comparisons of tomographic reconstruction techniques by analytical method using Bessel function and Zernicke polynomial as base functions for radial expansion have been done.

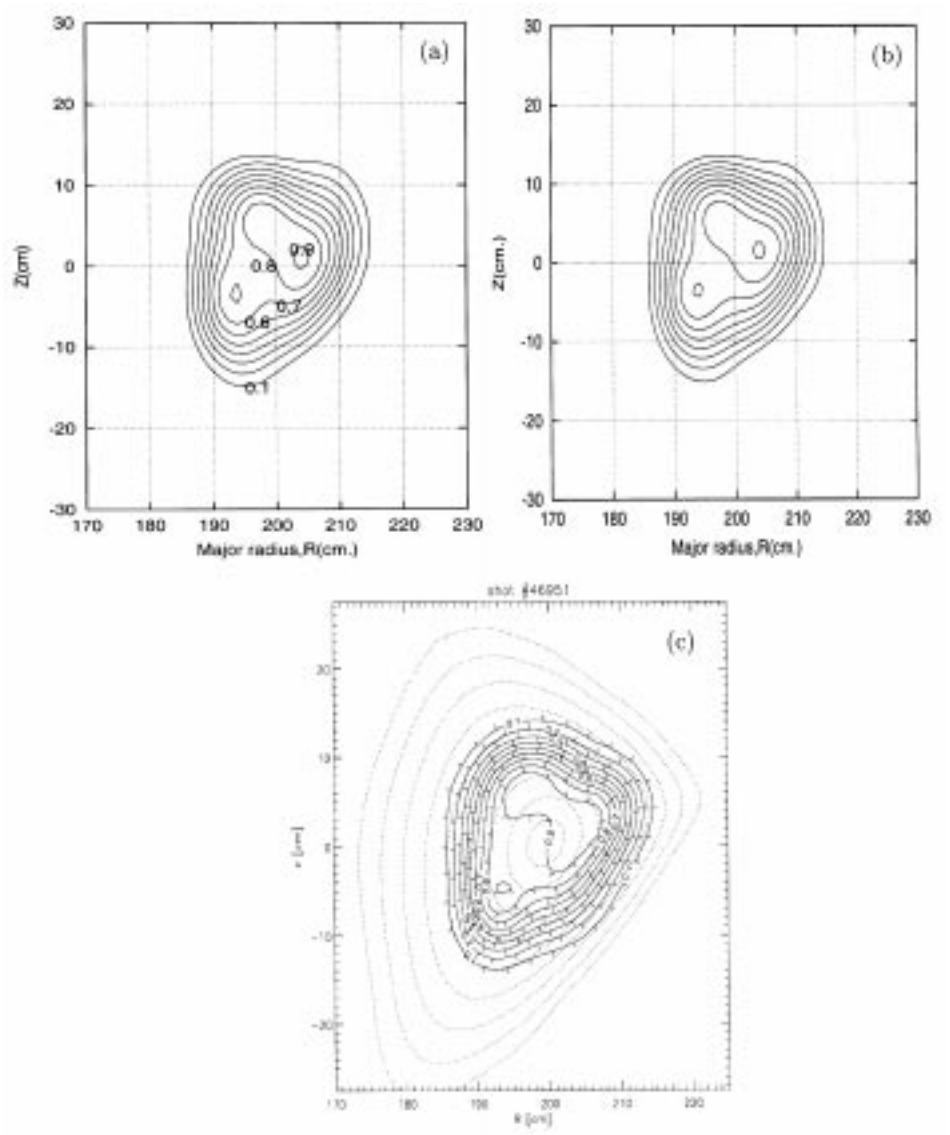

Figure 6. Reconstructed image of sxr emissivity of W7-AS Stellarator (**a**) using Bessel function as the base function for radial expansion, (**b**) using Zernicke polynomial as the base function for radial expansion and (**c**) is the reconstructed 2D image supplied by Weller and Klose [15].

The superiority of Bessel function as a base function over Zernicke polynomial is quite clear from the reconstructed images and the discussions in the previous section. It is obvious that without virtual chords tomography using Zernicke polynomial is not possible. Not only that, it takes more expansion terms than that using Bessel function in tomographic reconstruction. The W7-AS Stellarator data analysed by Weller and Klose have also been

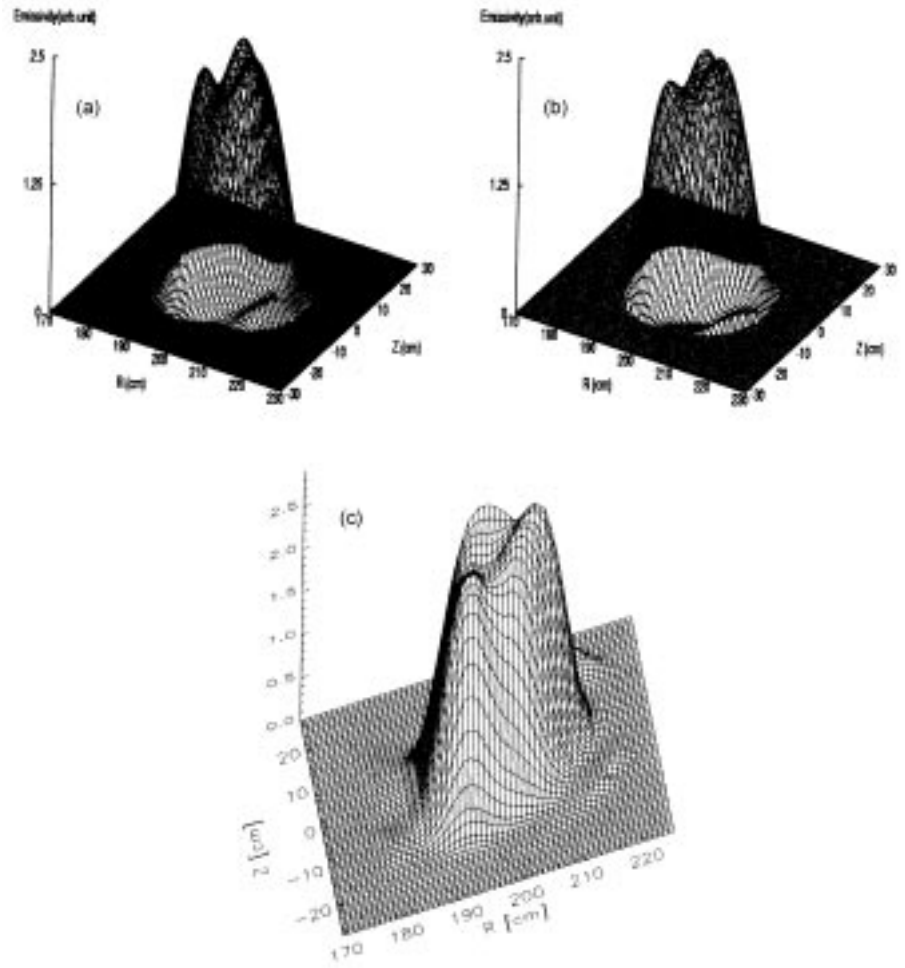

Figure 7. (**a**) The 3D image of the W7-AS Stellarator sxr data using Bessel function as the base function for radial expansion, (**b**) when Zernicke polynomial was used as base function and (**c**) 3D image supplied by Weller and Klose [15].

analysed by us. They have done the tomographic reconstruction by 'pixel method' using 'maximum entropy' constraint for regularization [6,19]. A comparison of our analysis using analytical method with 'pixel method' shows an excellent agreement. Our present work also shows that results do not sensitively depend upon the numerical approach.

Acknowledgement

One of us (AKC) is grateful to Arther Weller and Soeren Klose, Max-Planck-Institut fur Plasma Physik, Germany, for providing experimental data from W7-AS Stellarator and their critical evaluation of our analysis.

References

[1] P Smeulders, *Nucl. Fusion* **23**, 529 (1983)
[2] Y Nagayama, S Tsuji, K Kawahata and N Noda, *Jpn. J. Appl. Phys.* **20**, L779 (1981)
[3] R S Granetz and J M Camacho, *Nucl. Fusion* **25**, 727 (1985)
[4] R S Granetz and J M Camacho, *Rev. Sci. Instrum.* **57**, 417 (1986)
[5] R S Granetz and P Smeulders, *Nucl. Fusion* **28**, 457 (1988)
[6] A Weller, C Gorner and D Gonda, *Rev. Sci. Instrum.* **70**, 484 (1999)
[7] C G Windsor, T N Todd, D L Tortmann and M E U Smeth, *Fusion Technology* **32**, 416 (1997)
[8] J P Christiansen, J D Callen, J J Ellis and R S Granetz, *Nucl. Fusion* **29**, 703 (1989)
[9] W H Press, S A Teukolsky, W T Vetterling and B P Flannery (eds), *Numerical recipes in Fortran: The art of scientific computing*, 2nd ed. (Cambridge University Press, Cambridge, 1992)
[10] A M Cormack, *J. Appl. Phys.* **34**, 2722 (1963)
[11] A M Cormack, *J. Appl. Phys.* **35**, 2908 (1964)
[12] L Wang and R S Granetz, *Rev. Sci. Instrum.* **62**, 842 (1991)
[13] L Wang and R S Granetz, *Rev. Sci. Instrum.* **62**, 1115 (1991)
[14] M A Dubois, D A Marty and A Pochelon, *Nucl. Fusion* **20**, 1355 (1980)
[15] A Weller and Soren Klose, private communication (2000)
[16] A K Chattopadhyay, C V S Rao, S K Mattoo and R Srivatsan, Institute for Plasma Research, Technical Report IPR/TR-88/2002 (2002)
[17] A K Chattopadhyay, C V S Rao and R Srivatsan, Institute for Plasma Research, Research Report, IPR/RR-287/2002 (2002)
[18] Y C Saxena, SST-1 team, *Nucl. Fusion* **40**, 1069 (2000)
[19] M Anton, H Weisen, M J Dutch, W Vander Linden, F Buhlmann, R Chavan, B Marletaz, P Marmillod and P Paris, *Plasma Phys. Control. Fusion* **38**, 1849 (1996)